Ab initio description of the $Bi_2Sr_2CaCu_2O_{8+\delta}$ electronic structure

Johannes Nokelainen,[1,*] Christopher Lane,[2,3,†] Robert S. Markiewicz,[4] Bernardo Barbiellini,[1,4] Aki Pulkkinen,[5,1] Bahadur Singh,[4] Jianwei Sun,[6] Katariina Pussi,[1] and Arun Bansil[4]

[1] *Department of Physics, School of Engineering Science, LUT University, FI-53850 Lappeenranta, Finland*
[2] *Theoretical Division, Los Alamos National Laboratory, Los Alamos, New Mexico 87545, USA*
[3] *Center for Integrated Nanotechnologies, Los Alamos National Laboratory, Los Alamos, New Mexico 87545, USA*
[4] *Physics Department, Northeastern University, Boston, Massachusetts 02115, USA*
[5] *Département de Physique and Fribourg Center for Nanomaterials, Université de Fribourg, CH-1700 Fribourg, Switzerland*
[6] *Department of Physics and Engineering Physics, Tulane University, Louisiana 70118 New Orleans, USA*

(Received 26 March 2020; revised manuscript received 20 May 2020; accepted 21 May 2020; published 26 June 2020)

Bi-based cuprate superconductors are important materials for both fundamental research and applications. As in other cuprates, the superconducting phase in the Bi compounds lies close to an antiferromagnetic phase. Our density functional theory calculations based on the strongly-constrained-and-appropriately-normed exchange correlation functional in $Bi_2Sr_2CaCu_2O_{8+\delta}$ reveal the persistence of magnetic moments on the copper ions for oxygen concentrations ranging from the pristine phase to the optimally hole-doped compound. We also find the existence of ferrimagnetic solutions in the heavily doped compounds, which are expected to suppress superconductivity.

DOI: 10.1103/PhysRevB.101.214523

I. INTRODUCTION

In 1986 superconductivity above 30 K was reported in La_2CuO_4 by Bednorz and Müller [1], initiating an intense effort to understand its microscopic origin and gain insight into driving the T_c above the room temperature. The anomalous nature of the cuprate superconductivity is believed to originate from the quasi-two-dimensional CuO_2 planes wherein a strong long-range antiferromagnetic (AFM) order is found in the parent half-filled compound [2]. On doping, the AFM order quickly disappears and gives way to a superconducting dome. From this intimate connection between antiferromagnetism and superconductivity, the view that spin-fluctuations play a central role in determining the physical properties of the cuprates has been gaining increasing support [3–5]. However, there is still no universally accepted explanation for high-temperature superconductivity.

Crucial to understanding the origin of superconductivity in the cuprates is the process by which doped hole carriers are introduced into the CuO_2 planes. In simplified low-energy effective models, such as the one-band Hubbard model, only the Cu-*d* and O-*p* states are assumed to dominate. This view of the cuprates has been successful in describing the robust broken symmetry phases seen in experiments but it does not account for the diversity of transition temperatures at optimal doping. For example, the highest T_c obtained in $La_{2-x}Sr_xCuO_4$ is 40 K, whereas in the single-layer Hg cuprate, $HgBa_2CuO_4$, the optimal T_c is almost 100 K, more than twice that of $La_{2-x}Sr_xCuO_4$. These variations have been accounted for by modifying the local crystal-field splittings in the CuO_6 octahedra [6], which in turn alter fine features of the Fermi surface [7]. However, these models ignore impurity and structural effects derived from real dopants. Moreover, such models do not account for interlayer coupling effects between the CuO_2 planes and the charge-reservoir layers. Therefore, the doping process must be theoretically modeled in a holistic manner by treating the CuO_2 plane, the surrounding layers, and the dopants on the same footing.

The bismuth-based cuprates $Bi_2Sr_2Ca_{n-1}Cu_nO_{2n+4+\delta}$ (BSCCO) [8–12] are among the most extensively investigated superconductors. Notably, the weak van der Waals-like coupling between the layers, facilitates cleaving and makes BSCCO amenable to accurate angle resolved photoemission spectroscopy (ARPES) [13–21] and scanning-tunneling microscopy/spectroscopy (STM/STS) [22–31] studies. The two-layer compound ($n = 2$) is composed of a rock-salt SrO-BiO_δ-SrO charge reservoir layer stacked with two CuO_2-Ca-CuO_2 layers. Unlike the mercury- or yttrium-based cuprates, the oxygen impurities in BSCCO can occupy at least three distinct sites. These sites have been extensively studied with STM, and the findings have been compared to various models [32–34].

Initial theoretical studies of cuprates using the density functional theory (DFT) missed important Coulomb correlation effects [35]. In BSCCO, the local-spin-density-approximation (LSDA) fails to produce the copper magnetic moments [36–40]. The generalized-gradient-approximation (GGA) produces only marginal corrections to the LSDA [34,41–44]. Jarlborg has suggested applying higher-order density gradient corrections to cuprates [45]. Additional studies beyond the GGA using schemes such as DFT + U [46] and DFT + DMFT [47] have been performed to stabilize the AFM ground state. However, these methods

*johannes.nokelainen@lut.fi
†laneca@lanl.gov

require the use of external parameters such as the Hubbard U, which limits the predictive power of the theory.

Recent progress on advanced DFT schemes offers new pathways for describing the electronic structure of correlated materials from first principles. In particular, the strongly-constrained-and-appropriately-normed (SCAN) meta-GGA exchange-correlation functional [48], which obeys all known constraints applicable to meta-GGA, has been shown to accurately predict many of the key properties of pristine and doped La_2CuO_4 [49–51] and $YBa_2Cu_3O_6$ [52]. In La_2CuO_4, SCAN correctly captures the magnetic moment in magnitude and orientation, the magnetic exchange coupling parameter, and the magnetic form factor along with the electronic band gap, all in accord with the corresponding experimental results. Reference [51] compares SCAN with other meta-GGA and hybrid functionals in cuprates and shows that SCAN gives the best overall agreement with experiments. In a SCAN-based study, Ref. [52] identifies a landscape of 26 competing uniform and stripe phases in near-optimally doped $YBa_2Cu_3O_7$. In Ref. [52], the charge, spin and lattice degrees of freedom are treated on an equal footing in a fully self-consistent manner to show how stable stripe phases can be obtained without invoking any free parameters. These results indicate that SCAN correctly captures many key features of the electronic and magnetic structures of the cuprates and it thus provides a next-generation baseline for incorporating the missing many-body effects such as the quasiparticle lifetimes and waterfall features [53]. The applicability of SCAN to transition-metal oxides, semiconductors, and atomically thin films beyond graphene has been demonstrated in Refs. [54–62]. We note that SCAN also contains overcorrections to the GGA in dealing with itinerant ferromagnetism [63,64], but the underlying deficiencies responsible for these issues with SCAN have been identified and possible fixes have been proposed [65,66]. There is no evidence that these issues with SCAN persist outside of the ferromagnets, since SCAN clearly improves GGA in the case of antiferromagnetic α-Mn [67].

In this article, we utilize the SCAN functional to explore the electronic, structural and magnetic properties of $Bi_2Sr_2CaCu_2O_8$ (Bi2212) on a first-principles basis. A realistic description of the phase diagram of BSCCO requires also an accurate treatment of the self-doping by the BiO layers and a precise description of the oxygen interstitials, which can occupy different sites. We will show that a robust copper magnetic moment persists even when a substantial amount of oxygen is added to the material, which is in agreement with recent resonant inelastic x-ray spectroscopy (RIXS) experiments [68–71]. The appearance of the Cu magnetic moment in SCAN continues to capture other good trends seen in the LDA and GGA computations [40]. Finally, we find that SCAN predicts ferrimagnetic solutions in overdoped BSCCO in agreement with recent experiments by Kurashima *et al.* [72].

This paper is organized as follows. Section II discusses the methodology, where Sec. II A describes the computational details and Sec. II B considers the structural models for BSCCO. Section III presents the results of this study. Here, Sec. II A focuses on pristine Bi2212 while Secs. III B and III C present the results for oxygen-doped BSCCO with O impurities located at various positions in the lattice. Section IV summarizes our conclusions and comments on future implications of our work.

II. METHODOLOGY

A. Computational details

Ab initio calculations were carried out using the projector-augmented-wave method [73,74] as implemented in the Vienna *ab initio* simulation package [75,76]. The Kohn-Sham orbitals [77] were expanded in a plane-wave basis set with an energy cutoff of 550 eV. The exchange-correlation energy is treated within the SCAN meta-GGA scheme [48]. Some calculations were also carried out within the GGA scheme of Perdew, Burke, and Ernzerhof [78] for reference. All sites in the unit cell along with the unit cell dimensions were relaxed using a quasi-Newton algorithm to minimize energy with an atomic force tolerance of 0.001 eV/Å. A $9 \times 9 \times 2$ ($4 \times 4 \times 1$ k-mesh was used to sample the Brillouin zone of the bulk (slab) crystal structure and a denser $15 \times 15 \times 3$ k-mesh was employed to calculate the density of states (DOS). A total energy tolerance of 10^{-5} eV was used to determine the self-consistent charge density. The band structure was unfolded [79,80] from the supercell into the primitive cell Brillouin zone using the PyProcar [81] code. Various site-resolved projections were analyzed with the PYMATGEN [82] software package.

B. Structural model of BSCCO

An important characteristic of the cuprates is the presence of an intrinsic lattice mismatch between the various layers [83]. In BSCCO, the substantial tensile stress in the BiO layers leads to an incommensurate superlattice modulation [84] in which the CuO_2 and BiO layers undergo warping and rippling with an approximate period of five unit cells along the b axis. The reported effects of this supermodulation on the electronic properties have been mixed in that ARPES finds no effect on T_c as a function of superstructure period [85], whereas STM finds the local doping level to be connected to the periodicity of the structural modulations [86]. A few theoretical studies have been performed within the DFT [34,42] but clear conclusions have been difficult to obtain due to the intrinsic limitations of the LSDA and GGA.

In this study, we neglect the superstructure modulation and focus on the electronic and magnetic properties and their evolution with doping. In this connection, we consider a $\sqrt{2} \times \sqrt{2}$ orthorhombic supercell to accommodate the (π, π) AFM order on the copper atomic sites (see Fig. 1). After relaxing the atomic positions and unit-cell shape, we find the a, b, and c lattice parameters to be 5.35 Å, 5.42 Å, and 31.08 Å, respectively, admitting a 1.1 % orthorhombicity in the ab plane. These parameters are in good accord with the corresponding experimental results [$a = 5.399(2)$ Å, $b = 5.414(1)$ Å, and $c = 30.904(16)$ Å] [8]. Interestingly, in comparison to a freestanding BiO bilayer, our computations show that the BiO bilayer in BSCCO is under a tensile strain of 9.3 % due to lattice mismatch [87]. Consequently, the Bi and O ions rearrange themselves and exhibit stronger BiO bonding along the a axis compared to the b axis, yielding zig-zag BiO chains or Bi_2O_2 quadrilaterals [42,88,89]. The chain formation appears to be key for stabilizing the orthorhombic ground state.

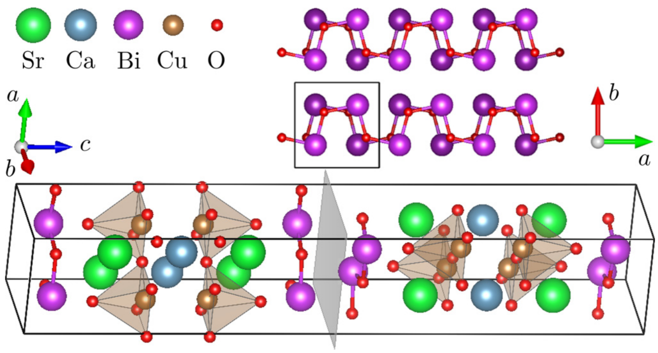

FIG. 1. A schematic of the relaxed orthorhombic $\sqrt{2} \times \sqrt{2}$ supercell structure of Bi2212 and the zigzag chains of BiO bilayers. This zigzag stacking configuration within the BiO bilayers yielded the lowest energy. The vdW gap in the BiO layer (highlighted with the gray plane) divides the structure into two slabs. Black lines mark the computational unit cell.

In order to delineate effects of doping, we doubled the unit cell in the *ab* plane. Since the bulk Bi2212 crystal consists of two formula units stacked body-center-wise and separated by a van der Waals (vdW) region with very little k_z dispersion [90], we followed previous computational studies [33,41,43] and considered only one formula unit. Using a small vacuum region of 3.8 Å to separate the periodic images of these slabs, we verified that the electronic properties of this simplified model correspond well to those of the bulk.

III. RESULTS

A. Electronic structure of pristine Bi2212

Figure 2 compares band structures and site-resolved partial-densities-of-states (PDOSs) of Bi2212 obtained within the GGA and SCAN schemes. Consistent with previous *ab initio* studies [40,43], GGA [Fig. 2(a)] yields a nonmagnetic metal, where the spin-degenerate Cu $d_{x^2-y^2}$ bands cross the Fermi level with an overall bandwidth of 4.0 eV. In contrast, SCAN [Fig. 2(b)] stabilizes the AFM order over the copper sublattice and produces an indirect gap of 0.33 eV in the half-filled $d_{x^2-y^2}$-dominated band. At the X point, the energy gap is 1.47 eV, while at the midpoint between M and Γ [91], the gap is 1.24 eV. When the band structure is projected onto the Cu ions with positive magnetic moments [Fig. 2(c)], the spin-polarized nature of the Cu $d_{x^2-y^2}$ bands become visible. The valence band (majority spin) is now seen to be partially occupied, while the conduction band (minority spin) is unoccupied, leading to local Cu magnetic moments of $\pm 0.425\,\mu_B$. Around X, the valence bands exhibit a bilayer splitting of 0.24 eV, which produces two van Hove singularities visible in the PDOS at around −0.65 eV and −0.88 eV. These singularities visually appear to be stronger than logarithmic, in agreement with Nieminen *et al.* [27]. The Cu d_{z^2} and t_{2g} orbitals are spin-split due to the Hund's coupling [see Fig. 2(b)]. This splitting is substantial for the d_{z^2} orbitals but weak for the t_{2g} orbitals; we find that the d_{z^2} orbitals contribute mainly between −1.7 eV and −2.2 eV in the spin up channel and between −2.7 eV and −3.2 eV in the spin down channel. In contrast, the t_{2g} majority and minority spin states are nearly degenerate, with the weight of $d_{xz/yz}$ orbitals concentrated between −1.7 eV and −1.0 eV, and that of d_{xy} orbitals between −2.0 eV and −1.2 eV. Hund's coupling leads to similar orbital splitting behavior in La_2CuO_4, but with different ordering of the d orbitals [49]. Here, the d_{z^2} bands are below the t_{2g} bands, whereas in La_2CuO_4 they are the highest fully occupied bands. This difference between Bi2212 and La_2CuO_4 is a consequence of the larger separation between the Cu ions and the apical oxygen atoms in Bi2212; 2.67 Å in our relaxed structure compared to 2.45 Å in La_2CuO_4 [49].

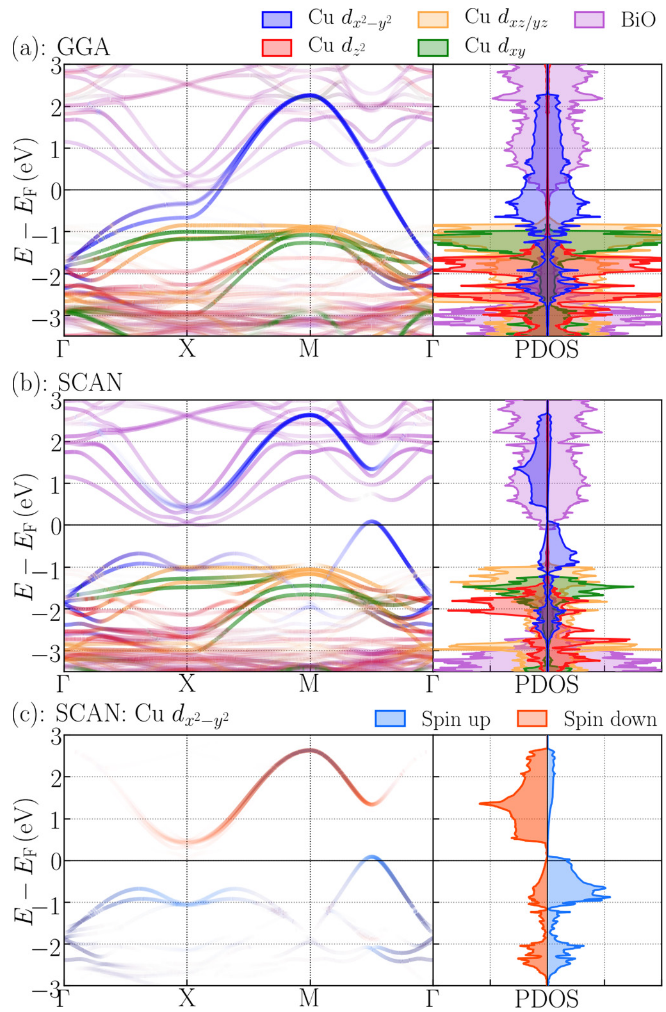

FIG. 2. [(a) and (b)] Band structure and DOS projected onto Cu d orbitals and BiO layers for GGA and SCAN. For SCAN, the Cu projections refer only to Cu ions with positive magnetic moments in order to highlight their spin polarization in PDOS (the total moment over the unit cell is zero). However, the spin polarization is not shown in the band structure plots for simplicity. (c): SCAN-based Cu $d_{x^2-y^2}$ bands and DOS. Here, spin polarization of the band structure is shown. Band structure has been unfolded [79,80] into the primitive cell from the AFM $\sqrt{2} \times \sqrt{2}$ supercell. X and M symmetry points are given with respect to the Brillouin zone of the primitive cell.

In order to estimate the value of on-site Hubbard potential U and the Hund's coupling J_H, we follow the approach of Lane *et al.* [49]. Using the PDOSs $g_{\mu\sigma}$ resolved by orbitals μ and spin σ, we determine the average spin-splitting

$\overline{E}_{\mu\sigma}$ of the $d_{x^2-y^2}$ and d_{z^2} levels and then U and J_H as follows:

$$\overline{E}_{\mu\sigma} = \int_W E g_{\mu\sigma}(E)\, dE, \quad (1)$$

$$\overline{E}_{d_{x^2-y^2}\uparrow} - \overline{E}_{d_{x^2-y^2}\downarrow} = U(N_\uparrow - N_\downarrow), \quad (2)$$

$$\overline{E}_{\mu\neq d_{x^2-y^2}\uparrow} - \overline{E}_{\mu\neq d_{x^2-y^2}\downarrow} = J_H(N_\uparrow - N_\downarrow), \quad (3)$$

where $N_\uparrow$ ($N_\downarrow$) is the occupation of the spin-up (down) $d_{x^2-y^2}$ orbital and the integration is over the full bandwidth W. In this way, U and $J_H(\mu = d_{z^2})$ are found to be 4.7 eV and 1.35 eV, respectively. These values are very similar to those found for La_2CuO_4 [49]. Also, this value of U is comparable to that found in the three-band Hubbard models of cuprates, but it is substantially larger than the U used in the single-band Hubbard model, which can be estimated through a constrained random phase approximation calculation [92] for Bi2212 [93] and $Bi_2Sr_2CuO_6$ (Bi2201) [70]. This difference is due to the over-simplified nature of the single-band model, where the band is composed of Cu-$d_{x^2-y^2}$ and O-p_x, p_y characters. This band thus essentially represents a CuO_2 molecule instead of a pure d state, so that the U estimated in this way involves partial screening by the O ligands.

The nearest-neighbor superexchange coupling parameter J is usually estimated by mapping to an effective Heisenberg model [49]. However, this is not possible here because we found that the ferromagnetic state in this case converges to zero magnetic moment. For this reason, we have used $J \approx 4t^2/U - 24t^4/U^3$, where t is the nearest-neighbor hopping parameter, which can be estimated from the $d_{x^2-y^2}$ bandwidth B to be $t = B/8 \approx 500$ meV. We thus estimate $J \approx 200$ meV, which is in reasonable accord with the corresponding experimental value of $\sim$148 meV [70].

Unlike the other cuprates such as La_2CuO_4, pristine BSCCO is weakly metallic due to self-doping [40]: Both the BiO and Cu $d_{x^2-y^2}$ bands cross E_F and lead to a semimetal through the removal of some electrons from the CuO plane. This self-doping effect may be the reason that it has been difficult to stabilize a large magnetic gap in nominally pristine BSCCO without rare-earth substitution [94,95]. We have also carried out computations on Bi2201 (see Supplementary Materials [96,97] for comparison of Bi2201 with Bi2212). Notably, the Cu magnetic moment in Bi2201 is found to be 0.395 μ_B, which is 0.030 μ_B less than in Bi2212. This reflects the effect of stronger self-doping in Bi2201 where the Bi/Cu ratio is twice as large as in Bi2212.

B. Doping of Bi2212

STM studies of Zeljkovic *et al.* [32,33] show that there are two different types of interstitial oxygen dopants in BSCCO. The "type B" dopants reside in the BiO layers, whereas the "type A" oxygens lie close to the apical oxygen atoms and the SrO layers and interact directly with the CuO_2 planes. We have modeled both types of these dopants and found that the type A oxygen dopants explain most of the observed hole-type doping. The B oxygen dopants are discussed further in Sec. III C below. Our calculations for modeling doping effects employed a 120-atom $2\sqrt{2} \times 2\sqrt{2}$ supercell slab (see Sec. II for details) with a type A interstitial oxygen atom O_{int}. This model corresponds to a doping level of $\delta = 1/8$ (close to optimal doping), as illustrated in Fig. 3(a). In the

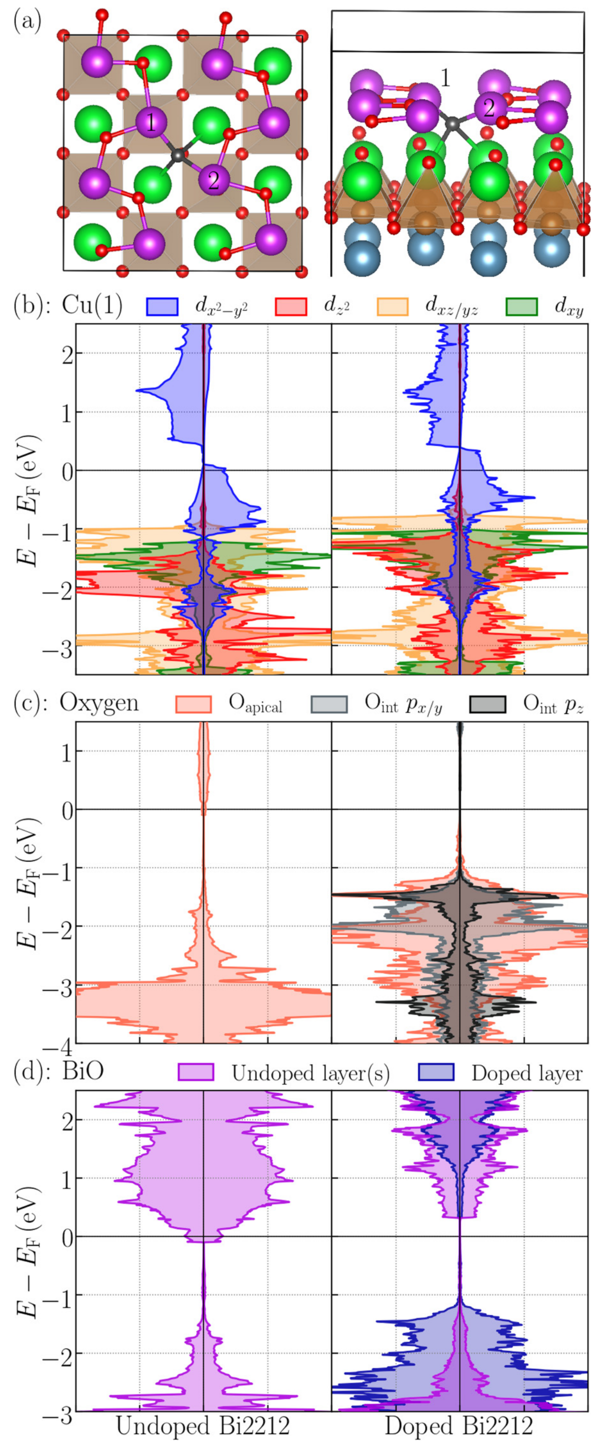

FIG. 3. (a) Top and side views of the relaxed Bi2212 slab with an type A-type O dopant. O_{int} is colored black. The Cu(1)/Cu(2) and the $O_{apical}(1)$/$O_{apical}(1)$ atoms are located below the Bi atoms labeled 1/2. (b) lm-decomposed PDOS of the Cu(1) ion [closest to O_{int}, see panel (a)] in pristine (left) and doped (right) cases. (c) p-projected PDOS of the $O_{apical}(1)$ atom with and without doping. For the doped case (right), the PDOS of the O_{int} is also presented. (d) PDOS projected onto the BiO layers.

relaxed structure the O_{int} atom is found to reside between the SrO and BiO layers in agreement with the results of He *et al.* [41,42] and Foyevtsova *et al.* [43] as well as with a recent scanning-transmission-electron microscopy (STEM) study by Song *et al.* [34].

In Fig. 3(b), we illustrate the effects of dopant on the electronic structure by comparing the pristine and doped PDOS on Cu(1) site, which is the copper ion closest to the O_{int}. Doping leads to addition of holes resulting into a downwards shift of the Fermi level in the magnetic $d_{x^2-y^2}$ band, along with the closing of the $d_{x^2-y^2}$ electronic gap. The doping leads to a reduction in the average value of the Cu magnetic moment ($|\overline{M}| = 0.347\,\mu_B$) by $0.078\,\mu_B$. Values of $|M|$ differ significantly between the two CuO_2 planes. We will refer to the CuO_2 planes with/without the dopant as "doped/undoped" planes. On the undoped plane, $|M| = 0.363\,\mu_B$, whereas on the doped plane, the magnetic moments are on average $0.328\,\mu_B$ with significant variations on Cu sites ($0.322\,\mu_B \leqslant |M| \leqslant 0.339\,\mu_B$). The on-site potential of about 4.8 eV, calculated from the Cu $d_{x^2-y^2}$ PDOS, is constant for all the Cu sites and remains almost unchanged from the pristine case.

Note that the O dopant here resides between the apical oxygen atoms $O_{apical}(1)$ and $O_{apical}(2)$ at distances of 2.61 Å and 2.66 Å, respectively [see Fig. 3(a)]. The O_{int} interacts with the Cu(1) d_{z^2} orbitals primarily through $O_{apical}(1)$. However, as discussed in Sec. III A, this interaction is suppressed in BSCCO compared to other cuprates due to the larger Cu–O_{apical} separation. Lack of hybridization in the pristine case can be seen by comparing the Cu(1) d_{z^2} and $O_{apical}(1)$ PDOSs on the left sides of Figs. 3(b) and 3(c). In the doped case, the coupling between the Cu(1)/Cu(2) ions and the $O_{apical}(1)/O_{apical}(2)$ atoms is significantly enhanced because of 0.18 Å reduction of their separations to 2.49 Å. Consequently, the $O_{apical}(1)$ states are lifted from below -3 eV to the energy interval of -3 eV to -1 eV, as shown in Fig. 3(c). This modified $O_{apical}(1)$ PDOS displays strong common features with the Cu(1) d_{z^2} states as illustrated in the right side of Fig. 3(b). These results indicate substantial doping-induced interactions between these atoms. On the Cu(1) ion, the effect of these interactions is to lift the d_{z^2} orbitals by $\sim$0.3 eV with respect to the t_{2g} orbitals, which can be seen by comparing their average energies computed with Eq. (1). In addition, the shape of the Cu(1) d_{z^2} PDOS experiences significant modification. However, the estimated Hund's splitting (1.38 eV) remains almost unchanged. The overall trends described above are also present on the other Cu sites in a less pronounced form.

The right side of Fig. 3(c) gives insight into the nature of O_{int} PDOS. By comparing PDOSs of O_{int} and $O_{apical}(1)$ we see that both $p_{x/y}$ and p_z orbitals of O_{int} couple with $O_{apical}(1)$, with p_z coupling around -1.4 eV and $p_{x/y}$ around -2.0 eV. The O_{int} p_z PDOS is especially relevant for STM experiments since the tunneling involves the p_z orbital while the p_x/p_y orbitals are orthogonal to the STM tip [98]. Indeed, STM studies by Zeljkovic *et al.* [32,33] report a peak in the scanning-tunneling spectrum at -1.5 eV for the type A interstitial, which is close to the aforementioned O_{int} p_z PDOS peak at -1.4 eV.

Figure 3(d) shows the BiO-layer PDOS with and without the dopants. Doping is seen to lift the BiO bands above E_F in accord with the study of Lin *et al.* [40] and Bi2223 study of Camargo-Martínez *et al.* [44] where doping was done with Pb instead of O. Note that BiO pockets are removed also from BiO layer which does not lie close to the O_{int} although effects of dopant on this "undoped" layer are relatively weak. In contrast, the dopant induces substantial effects on the electronic states from the "doped" BiO layer (i.e. the layer close to O_{int}) where the spectral weights associated with the BiO states are lifted upwards by more than 1 eV and the BiO bands now overlap the Cu d bands in energy.

We also investigated the heavily overdoped regime ($\delta = 1/4$) by introducing a second type-A dopant that was placed in the structure as far as possible from the first dopant. Compared to $\delta = 1/8$, the average value of $|M|$ of the Cu ions in the overdoped case is lowered by $0.078\,\mu_B$ to $0.268\,\mu_B$. Interestingly, the higher doping also leads to the onset of ferrimagnetic order with average spin up/down moments on Cu atoms of $0.307\,\mu_B/-0.229\,\mu_B$. Moreover, the oxygen atoms in the CuO_2 planes now develop a magnetic moment of $+0.010\,\mu_B$. The total magnetization of the unit cell is $0.059\,\mu_B$ per copper. Such magnetization has been predicted to destroy superconductivity in overdoped cuprates [72,99,100].

C. Type B oxygen dopants

Following the experimental results of Zeljkovic *et al.* [32,33] and the computational study of He *et al.* [41], we placed the-type B oxygen dopants in the middle of the approximately square Bi network (position #2 of He *et al.*). This location is quite close to one of the oxygen atoms in the BiO layer and leads to the formation of an oxygen molecule as shown in Fig. 4(a). We find the bond length of this oxygen dimer to be 1.476 Å, which is close to the $[O_2]^{2-}$ bond length in BaO_2 of 1.49 Å [101]. This O_{int} stabilizes into a position slightly below the BiO layer, while the oxygen which it is attached lies above the BiO layer, so that the dimer is tilted by an angle of 33° from the c axis. The total energy of the type B-doped compound was found to be 2.27 eV higher than that of the type A-doped structure.

In contrast to our results for the type A interstitial O atom, we found that the B interstitials produce only little doping, with the Cu magnetic moments being decreased only by $0.014\,\mu_B$ to $0.402\,\mu_B$. The Cu $d_{x^2-y^2}$ state remains nearly unchanged, as seen from the PDOS in Fig. 4(b), and the BiO pocket is not lifted above E_F, as illustrated in Fig. 4(d). In the PDOS of the O_{int}, a clear peak appears at around -2.6 eV. This feature is also reflected in the PDOS of the O_{apical} [see Fig. 4(c)] and in the PDOS of the Cu d_{z^2} [see Fig. 4(b)], indicating that some interactions occur also between the type B O_{int} and the CuO_2 plane.

We also tested the interstitial oxygen position in the van der Waals gap between the BiO layers. The energy of this configuration was found to be between that of type A and B oxygen atoms. To the best of our knowledge, this impurity position has not been considered in the literature. A possible explanation is that these oxygen atoms are very mobile and therefore they disappear during the annealing of the material or combine with existing oxygens in the BiO layer to become type B oxygens. Additionally, they might be more sensitive to

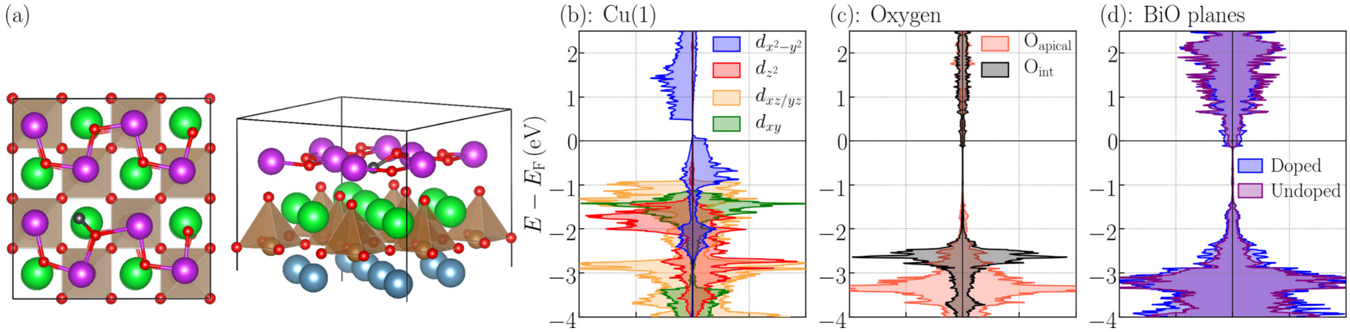

FIG. 4. (a) Structural model of a type B O-dopant in Bi2212. O_{int} is colored black. (b) PDOS of various d orbitals of a copper atom close to the O_{int}. (c) PDOS of the p orbitals of the O_{int} and an apical oxygen atom close to the dopant. (d) PDOS projected onto the BiO layers with and without the dopant.

the supermodulation distortions, which are not considered in our structural model.

IV. SUMMARY AND CONCLUSIONS

We have discussed the electronic structure of BSCCO compounds using accurate first-principles computations based on the SCAN functional, which does not require the introduction of any arbitrary parameters (e.g., the Hubbard U) to describe Coulomb correlation effects. As in our previous investigations of various cuprates, SCAN is found to greatly improve the description of the electronic states in the BSCCO system. In particular, our results yield accurate lattice geometries, copper magnetic moments and band structures that are in better agreement with experiments than GGA. The copper magnetic moments exhibit an antiferromagnetic coupling with and without oxygen dopants in accord with RIXS measurements, suggesting that superconductivity could be connected with quasiparticles coupled to spin fluctuations [5]. Oxygen dopants are shown to increase the coupling between the apical oxygens and the CuO_2 layers and modify especially the Cu d_{z^2} states. We also find the appearance of a doping-induced ferrimagnetic order that could be responsible for the suppression of superconductivity in the overdoped regime. The competition between superconductivity and ferrimagnetism hints that further studies of overdoped BSCCO could clarify important open questions such as the observation of a second dome of higher temperature superconductivity in the cuprates [102].

ACKNOWLEDGMENTS

It is a pleasure to acknowledge important discussions with Giacomo Ghiringhelli, Marco Moretti, and Xingjiang Zhou. The authors acknowledge CSC-IT Center for Science, Finland, for computational resources. J.N. is supported by the Finnish Cultural Foundation. The work at Northeastern University was supported by the US Department of Energy (DOE), Office of Science, Basic Energy Sciences Grant No. DE-FG02-07ER46352 (core research) and benefited from Northeastern University's Advanced Scientific Computation Center (ASCC), the NERSC supercomputing center through DOE Grant No. DE-AC02-05CH11231, and support (testing efficacy of advanced functionals) from the DOE EFRC: Center for Complex Materials from First Principles (CCM) under Grant No. DE-SC0012575. C.L. was supported by the US DOE NNSA under Contract No. 89233218CNA000001 and by the Center for Integrated Nanotechnologies, a DOE BES user facility, in partnership with the LANL Institutional Computing Program for computational resources. Additional support was provided by DOE Office of Basic Energy Sciences Program E3B5. B.B. acknowledges support from the COST Action CA16218. A.P. acknowledges the Osk. Huttunen Foundation for financial support. J.S. was supported by the US Department of Energy under EPSCoR Grant No. DE-SC0012432 with additional support from the Louisiana Board of Regents.

[1] J. G. Bednorz and K. A. Müller, Z. Phys. B Condens. Matter **64**, 189 (1986).
[2] J. M. Tranquada, G. Xu, and I. A. Zaliznyak, J. Magn. Magn. Mater. **350**, 148 (2014).
[3] D. J. Scalapino, E. Loh, and J. E. Hirsch, Phys. Rev. B **34**, 8190 (1986).
[4] D. J. Scalapino, Phys. Rep. **250**, 329 (1995).
[5] D. J. Scalapino, Rev. Mod. Phys. **84**, 1383 (2012).
[6] E. Pavarini, I. Dasgupta, T. Saha-Dasgupta, O. Jepsen, and O. K. Andersen, Phys. Rev. Lett. **87**, 047003 (2001).
[7] H. Sakakibara, H. Usui, K. Kuroki, R. Arita, and H. Aoki, Phys. Rev. Lett. **105**, 057003 (2010).
[8] M. A. Subramarian, C. C. Torardi, J. C. Calabrese, J. Gopalakrishnan, K. J. Morrissey, T. R. Askew, R. B. Flippen, U. Chowdhry, and A. W. Sleight, Science **239**, 1015 (1988).
[9] J. M. Tarascon, Y. LePage, L. H. Greene, B. G. Bagley, P. Barboux, D. M. Hwang, G. W. Hull, W. R. McKinnon, and M. Giroud, Phys. Rev. B **38**, 2504 (1988).
[10] J. M. Tarascon, W. R. McKinnon, P. Barboux, D. M. Hwang, B. G. Bagley, L. H. Greene, G. W. Hull, Y. LePage, N. Stoffel, and M. Giroud, Phys. Rev. B **38**, 8885 (1988).
[11] E. Sterpetti, J. Biscaras, A. Erb, and A. Shukla, Nat. Commun. **8**, 2060 (2017).

[12] S. Y. Frank Zhao, N. Poccia, M. G. Panetta, C. Yu, J. W. Johnson, H. Yoo, R. Zhong, G. D. Gu, K. Watanabe, T. Taniguchi, S. V. Postolova, V. M. Vinokur, and P. Kim, Phys. Rev. Lett. **122**, 247001 (2019).

[13] P. Aebi, J. Osterwalder, P. Schwaller, L. Schlapbach, M. Shimoda, T. Mochiku, and K. Kadowaki, Phys. Rev. Lett. **72**, 2757 (1994).

[14] N. L. Saini, J. Avila, A. Biaconi, A. Lanzara, M. C. Asensio, S. Tajima, G. D. Gu, and N. Koshizuka, Phys. Rev. Lett. **79**, 3467 (1997).

[15] H. Ding, J. R. Engelbrecht, Z. Wang, J. C. Campuzano, S.-C. Wang, H.-B. Yang, R. Rogan, T. Takahashi, K. Kadowaki, and D. G. Hinks, Phys. Rev. Lett. **87**, 227001 (2001).

[16] K. M. Lang, V. Madhavan, J. E. Hoffman, E. W. Hudson, H. Eisaki, S. Uchida, and J. C. Davis, Nature **415**, 412 (2002).

[17] A. Damascelli, Z. Hussain, and Z.-X. Shen, Rev. Mod. Phys. **75**, 473 (2003).

[18] T. L. Miller, M. Ärrälä, C. L. Smallwood, W. Zhang, H. Hafiz, B. Barbiellini, K. Kurashima, T. Adachi, Y. Koike, H. Eisaki, M. Lindroos, A. Bansil, D.-H. Lee, and A. Lanzara, Phys. Rev. B **91**, 085109 (2015).

[19] K. Gotlieb, C.-Y. Lin, M. Serbyn, W. Zhang, C. L. Smallwood, C. Jozwiak, H. Eisaki, Z. Hussain, A. Vishwanath, and A. Lanzara, Science **362**, 1271 (2018).

[20] Y. Ding, L. Zhao, H.-T. Yan, Q. Gao, J. Liu, C. Hu, J.-W. Huang, C. Li, Y. Xu, Y.-Q. Cai *et al.*, Chin. Phys. Lett. **36**, 017402 (2019).

[21] P. Ai, Q. Gao, J. Liu, Y. Zhang, C. Li, J. Huang, C. Song, H. Yan, L. Zhao, G.-D. Liu *et al.*, Chin. Phys. Lett. **36**, 067402 (2019).

[22] B. Barbiellini, O. Fischer, M. Peter, C. Renner, and M. Weger, Physica C **220**, 55 (1994).

[23] K. McElroy, R. W. Simmonds, J. E. Hoffman, D.-H. Lee, J. Orenstein, H. Eisaki, S. Uchida, and J. C. Davis, Nature **422**, 592 (2003).

[24] A. C. Fang, L. Capriotti, D. J. Scalapino, S. A. Kivelson, N. Kaneko, M. Greven, and A. Kapitulnik, Phys. Rev. Lett. **96**, 017007 (2006).

[25] O. Fischer, M. Kugler, I. Maggio-Aprile, C. Berthod, and C. Renner, Rev. Mod. Phys. **79**, 353 (2007).

[26] L. Dudy, C. Janowitz, O. Lübben, B. Müller, A. Ariffin, A. Krapf, H. Dwelk, and R. Manzke, J. Supercond. Nov. Magn. **22**, 51 (2009).

[27] J. Nieminen, I. Suominen, T. Das, R. S. Markiewicz, and A. Bansil, Phys. Rev. B **85**, 214504 (2012).

[28] P. Mistark, R. S. Markiewicz, and A. Bansil, Phys. Rev. B **91**, 140501(R) (2015).

[29] C.-T. Kuo, S.-C. Lin, G. Conti, S.-T. Pi, L. Moreschini, A. Bostwick, J. Meyer-Ilse, E. Gullikson, J. B. Kortright, S. Nemšák, J. E. Rault, P. Le Fèvre, F. Bertran, A. F. Santander-Syro, I. A. Vartanyants, W. E. Pickett, R. Saint-Martin, A. Taleb-Ibrahimi, and C. S. Fadley, Phys. Rev. B **98**, 155133 (2018).

[30] H. Li, X. Zhou, S. Parham, T. J. Reber, H. Berger, G. B. Arnold, and D. S. Dessau, Nat. Commun. **9**, 1 (2018).

[31] Y. Yu, L. Ma, P. Cai, R. Zhong, C. Ye, J. Shen, G. D. Gu, X. H. Chen, and Y. Zhang, Nature **575**, 156 (2019).

[32] I. Zeljkovic, Z. Xu, J. Wen, G. Gu, R. S. Markiewicz, and J. E. Hoffman, Science **337**, 320 (2012).

[33] I. Zeljkovic, J. Nieminen, D. Huang, T.-R. Chang, Y. He, H.-T. Jeng, Z. Xu, J. Wen, G. Gu, H. Lin, R. S. Markiewicz, A. Bansil, and J. E. Hoffman, Nano Lett. **14**, 6749 (2014).

[34] D. Song, X. Zhang, C. Lian, H. Liu, I. Alexandrou, I. Lazić, E. G. T. Bosch, D. Zhang, L. Wang, R. Yu, Z. Cheng, C. Song, X. Ma, W. Duan, Q. Xue, and J. Zhu, Adv. Funct. Mater. **29**, 1903843 (2019).

[35] W. E. Pickett, Rev. Mod. Phys. **61**, 433 (1989).

[36] S. Massidda, J. Yu, and A. Freeman, Physica C **152**, 251 (1988).

[37] L. F. Mattheiss and D. R. Hamann, Phys. Rev. B **38**, 5012 (1988).

[38] M. S. Hybertsen and L. F. Mattheiss, Phys. Rev. Lett. **60**, 1661 (1988).

[39] L. P. Chan, D. R. Harshman, K. G. Lynn, S. Massidda, and D. B. Mitzi, Phys. Rev. Lett. **67**, 1350 (1991).

[40] H. Lin, S. Sahrakorpi, R. S. Markiewicz, and A. Bansil, Phys. Rev. Lett. **96**, 097001 (2006).

[41] Y. He, T. S. Nunner, P. J. Hirschfeld, and H.-P. Cheng, Phys. Rev. Lett. **96**, 197002 (2006).

[42] Y. He, S. Graser, P. J. Hirschfeld, and H.-P. Cheng, Phys. Rev. B **77**, 220507(R) (2008).

[43] K. Foyevtsova, H. C. Kandpal, H. O. Jeschke, S. Graser, H.-P. Cheng, R. Valentí, and P. J. Hirschfeld, Phys. Rev. B **82**, 054514 (2010).

[44] J. Camargo-Martínez, D. Martínez-Pieschacón, and R. Baquero, Physica C **535**, 34 (2017).

[45] T. Jarlborg, Adv. Condens. Matter Phys. **2010**, 912067 (2009).

[46] V. I. Anisimov, J. Zaanen, and O. K. Andersen, Phys. Rev. B **44**, 943 (1991).

[47] C. Weber, Sci. Bull. **62**, 102 (2017).

[48] J. Sun, A. Ruzsinszky, and J. P. Perdew, Phys. Rev. Lett. **115**, 036402 (2015).

[49] C. Lane, J. W. Furness, I. G. Buda, Y. Zhang, R. S. Markiewicz, B. Barbiellini, J. Sun, and A. Bansil, Phys. Rev. B **98**, 125140 (2018).

[50] J. W. Furness, Y. Zhang, C. Lane, I. G. Buda, B. Barbiellini, R. S. Markiewicz, A. Bansil, and J. Sun, Commun. Phys. **1**, 11 (2018).

[51] K. Pokharel, C. Lane, J. W. Furness, R. Zhang, J. Ning, B. Barbiellini, R. S. Markiewicz, Y. Zhang, A. Bansil, and J. Sun, arXiv:2004.08047 (2020).

[52] Y. Zhang, C. Lane, J. W. Furness, B. Barbiellini, J. P. Perdew, R. S. Markiewicz, A. Bansil, and J. Sun, Proc. Natl. Acad. Sci. USA **117**, 68 (2020).

[53] T. Das, R. Markiewicz, and A. Bansil, Adv. Phys. **63**, 151 (2014).

[54] J. Varignon, M. Bibes, and A. Zunger, Phys. Rev. B **100**, 035119 (2019).

[55] Y. Zhang, J. Furness, R. Zhang, Z. Wang, A. Zunger, and J. Sun, arXiv:1906.06467 (2019).

[56] H. Hafiz, K. Suzuki, B. Barbiellini, Y. Orikasa, S. Kaprzyk, N. Tsuji, K. Yamamoto, A. Terasaka, K. Hoshi, Y. Uchimoto, Y. Sakurai, H. Sakurai, and A. Bansil, Phys. Rev. B **100**, 205104 (2019).

[57] J. Sun, R. C. Remsing, Y. Zhang, Z. Sun, A. Ruzsinszky, H. Peng, Z. Yang, A. Paul, U. Waghmare, X. Wu, M. L. Klein, and J. P. Perdew, Nat. Chem. **8**, 831 (2016).

[58] R. Car, Nat. Chem. **8**, 820 (2016).

[59] I. G. Buda, C. Lane, B. Barbiellini, A. Ruzsinszky, J. Sun, and A. Bansil, Sci. Rep. **7**, 44766 (2017).
[60] E. B. Isaacs and C. Wolverton, Phys. Rev. Mater. **2**, 063801 (2018).
[61] Y. Zhang, D. A. Kitchaev, J. Yang, T. Chen, S. T. Dacek, R. A. Sarmiento-Pérez, M. A. L. Marques, H. Peng, G. Ceder, J. P. Perdew, and J. Sun, Npj Comput. Mater. **4**, 9 (2018).
[62] C. Lane, Y. Zhang, J. W. Furness, R. S. Markiewicz, B. Barbiellini, J. Sun, and A. Bansil, Phys. Rev. B **101**, 155110 (2020).
[63] Y. Fu and D. J. Singh, Phys. Rev. Lett. **121**, 207201 (2018).
[64] F. Tran, G. Baudesson, J. Carrete, G. K. H. Madsen, P. Blaha, K. Schwarz, and D. J. Singh, arXiv:2004.04543 (2020).
[65] J. W. Furness and J. Sun, Phys. Rev. B **99**, 041119(R) (2019).
[66] D. Mejía-Rodríguez and S. B. Trickey, Phys. Rev. B **100**, 041113(R) (2019).
[67] A. Pulkkinen, B. Barbiellini, J. Nokelainen, V. Sokolovskiy, D. Baigutlin, O. Miroshkina, M. Zagrebin, V. Buchelnikov, C. Lane, R. S. Markiewicz, A. Bansil, J. Sun, K. Pussi, and E. Lähderanta, Phys. Rev. B **101**, 075115 (2020).
[68] M. Guarise, B. D. Piazza, H. Berger, E. Giannini, T. Schmitt, H. M. Rønnow, G. A. Sawatzky, J. van den Brink, D. Altenfeld, I. Eremin, and M. Grioni, Nat. Commun. **5**, 5760 (2014).
[69] Y. Y. Peng, M. Salluzzo, X. Sun, A. Ponti, D. Betto, A. M. Ferretti, F. Fumagalli, K. Kummer, M. Le Tacon, X. J. Zhou, N. B. Brookes, L. Braicovich, and G. Ghiringhelli, Phys. Rev. B **94**, 184511 (2016).
[70] Y. Y. Peng, G. Dellea, M. Minola, M. Conni, A. Amorese, D. Di Castro, G. M. De Luca, K. Kummer, M. Salluzzo, X. Sun, X. J. Zhou, G. Balestrino, M. Le Tacon, B. Keimer, L. Braicovich, N. B. Brookes, and G. Ghiringhelli, Nat. Phys. **13**, 1201 (2017).
[71] Y. Y. Peng, E. W. Huang, R. Fumagalli, M. Minola, Y. Wang, X. Sun, Y. Ding, K. Kummer, X. J. Zhou, N. B. Brookes, B. Moritz, L. Braicovich, T. P. Devereaux, and G. Ghiringhelli, Phys. Rev. B **98**, 144507 (2018).
[72] K. Kurashima, T. Adachi, K. M. Suzuki, Y. Fukunaga, T. Kawamata, T. Noji, H. Miyasaka, I. Watanabe, M. Miyazaki, A. Koda, R. Kadono, and Y. Koike, Phys. Rev. Lett. **121**, 057002 (2018).
[73] P. E. Blöchl, Phys. Rev. B **50**, 17953 (1994).
[74] G. Kresse and D. Joubert, Phys. Rev. B **59**, 1758 (1999).
[75] G. Kresse and J. Furthmüller, Comput. Mater. Sci. **6**, 15 (1996).
[76] G. Kresse and J. Furthmüller, Phys. Rev. B **54**, 11169 (1996).
[77] W. Kohn, Rev. Mod. Phys. **71**, 1253 (1999).
[78] J. P. Perdew, K. Burke, and M. Ernzerhof, Phys. Rev. Lett. **77**, 3865 (1996).
[79] P. B. Allen, T. Berlijn, D. A. Casavant, and J. M. Soler, Phys. Rev. B **87**, 085322 (2013).
[80] P. V. C. Medeiros, S. Stafström, and J. Björk, Phys. Rev. B **89**, 041407(R) (2014).
[81] U. Herath, P. Tavadze, X. He, E. Bousquet, S. Singh, F. Muñoz, and A. H. Romero, Comput. Phys. Commun. **251**, 107080 (2020).
[82] S. P. Ong, W. D. Richards, A. Jain, G. Hautier, M. Kocher, S. Cholia, D. Gunter, V. L. Chevrier, K. A. Persson, and G. Ceder, Comput. Mater. Sci. **68**, 314 (2013).
[83] E. Dagotto, Science **309**, 257 (2005).
[84] N. Poccia, G. Campi, M. Fratini, A. Ricci, N. L. Saini, and A. Bianconi, Phys. Rev. B **84**, 100504(R) (2011).
[85] L. Jing, Z. Lin, G. Qiang, A. Ping, Z. Lu, X. Tao, H. Jian-Wei, D. Ying, H. Cheng, Y. Hong-Tao, S. Chun-Yao, X. Yu, L. Cong, C. Yong-Qing, R. Hong-Tao, W. Ding-Song, L. Guo-Dong, W. Qing-Yan, H. Yuan, Z. Feng-Feng, Y. Feng, P. Qin-Jun, L. Shi-Liang, Y. Huai-Xin, L. Jian-Qi, X. Zu-Yan, and X.-J. Zhou, Chin. Phys. B **28**, 077403 (2019).
[86] C. Zou, Z. Hao, H. Li, X. Li, S. Ye, L. Yu, C. Lin, and Y. Wang, Phys. Rev. Lett. **124**, 047003 (2020).
[87] We are not aware of experimental lattice parameters for a freestanding BiO bilayer in the literature.
[88] W. Fan and Z. Zeng, Supercond. Sci. Technol. **24**, 105007 (2011).
[89] I. Zeljkovic, E. J. Main, T. L. Williams, M. C. Boyer, K. Chatterjee, W. D. Wise, Y. Yin, M. Zech, A. Pivonka, T. Kondo, T. Takeuchi, H. Ikuta, J. Wen, Z. Xu, G. D. Gu, E. W. Hudson, and J. E. Hoffman, Nat. Mater. **11**, 585 (2012).
[90] We studied the k_z dispersion of the electronic structure by looking along the $(0,0,0)-(0,0,\frac{\pi}{2})$ and $(\frac{\pi}{2},\frac{\pi}{2},0)-(\frac{\pi}{2},\frac{\pi}{2},\frac{\pi}{2})$ paths in the AFM BZ and we found no significant dispersion.
[91] In the supercell BZ this point corresponds to the X-point, and the primitive cell X-point corresponds to the supercell M point.
[92] S. W. Jang, H. Sakakibara, H. Kino, T. Kotani, K. Kuroki, and M. J. Han, Sci. Rep. **6**, 33397 (2016).
[93] S.-L. Yang, J. A. Sobota, Y. He, Y. Wang, D. Leuenberger, H. Soifer, M. Hashimoto, D. H. Lu, H. Eisaki, B. Moritz, T. P. Devereaux, P. S. Kirchmann, and Z.-X. Shen, Phys. Rev. B **96**, 245112 (2017).
[94] A. Moudden, L. Vasiliu-Doloc, N. Blanchard, G. Collin, and J. Hammann, Physica C **235–240**, 1621 (1994).
[95] V. P. S. Awana, L. Menon, and S. K. Malik, Phys. Rev. B **51**, 9379 (1995).
[96] See Supplementary Material at http://link.aps.org/supplemental/10.1103/PhysRevB.101.214523 for comparison of Bi2201 with Bi2212 both in the article and in the online description?
[97] K. Imai, I. Nakai, T. Kawashima, S. Sueno, and A. Ono, Jpn. J. Appl. Phys. **27**, L1661 (1988).
[98] I. Suominen, J. Nieminen, R. S. Markiewicz, and A. Bansil, Phys. Rev. B **84**, 014528 (2011).
[99] A. Kopp, A. Ghosal, and S. Chakravarty, Proc. Natl. Acad. Sci. USA **104**, 6123 (2007).
[100] B. Barbiellini and T. Jarlborg, Phys. Rev. Lett. **101**, 157002 (2008).
[101] L. Sutton, *Tables of Interatomic Distances and Configuration in Molecules and Ions* (The Chemical Society, London, 1958).
[102] L. Deng, Y. Zheng, Z. Wu, S. Huyan, H.-C. Wu, Y. Nie, K. Cho, and C.-W. Chu, Proc. Natl. Acad. Sci. USA **116**, 2004 (2019).